Supporting Information for

High-Throughput Characterization of Single-Quantum-Dot Emission Spectra and Spectral Diffusion by Multi-Particle Spectroscopy

*Mark J. J. Mangnus[1], Jur W. de Wit[1], Sander J.W. Vonk[1], Jaco J. Geuchies[2], Wiebke Albrecht[3,4], Sara Bals[3,4], Arjan J. Houtepen[2] and Freddy T. Rabouw[1]**

[1] Debye Institute for Nanomaterials Science, Utrecht University
Princetonplein 1, 3584CC Utrecht, The Netherlands

[2] Optoelectronic Materials Section, Faculty of Applied Sciences, Delft University of Technology, van der Maasweg 9, 2629 HZ Delft, The Netherlands

[3] EMAT, University of Antwerp, Groenenborgerlaan 171, 2020 Antwerp, Belgium

[4] NANOlab Center of Excellence, University of Antwerp, 2020 Antwerp, Belgium

* Corresponding author. E-mail: f.t.rabouw@uu.nl

Section S1: Ensemble absorption and emission spectra

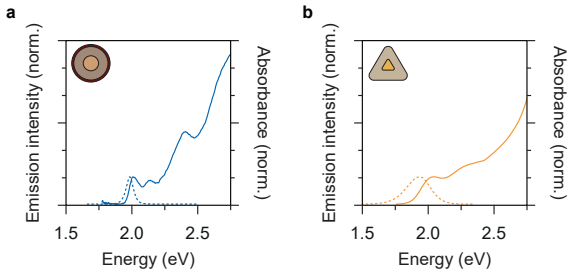

Figure S1 | Ensemble absorption and emission spectra. **(a)** Ensemble absorption (solid line) and emission spectrum (dashed line) of the CdSe/CdS/ZnS QDs. **(b)** Same, but for the InP/ZnSe QDs. The emission spectra have a fwhm of 70.7 meV (CdSe/CdS/ZnS) and 224 meV (InP/ZnSe). Emission spectra were recorded for a layer of QDs excited at 445 nm (CW) under the same conditions as we used for multi-particle spectroscopy experiments.

Section S2: Particle identification and background subtraction

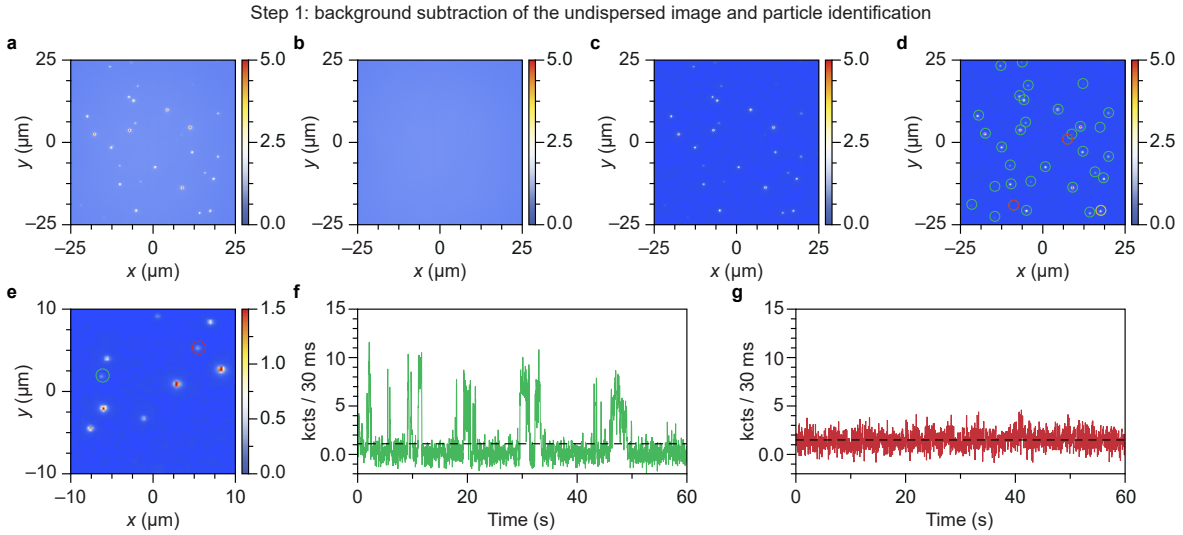

Figure S2 | Procedure of particle identification and background subtraction of CdSe/CdS/ZnS QDs (a) Non-dispersed image of 10–100 CdSe/CdS/ZnSe quantum dots (QDs), obtained by integrating a video over 60 s. A single QD emitter appears as a bright spot. QD positions are found by identifying isolated clusters of pixels with a high measured intensity. Color scale bars represent average count rates (in kcts / 25 ms). **(b)** Map of the background intensity, calculated by taking a moving average over 25 pixel intensities in the vertical direction, excluding pixels corresponding to QD positions. **(c)** Corrected 0^{th}-order image, obtained by subtracting the background. **(d–e)** Identification of QD positions. An initial guess of QD positions is based on pixel intensities. Bright positions (green circles) always correspond to a QD (or a cluster of QDs), while identification of QDs on some of the "dimmer" positions is less certain (red circles). Panel **e** is a zoom-in of panel **d**. **(f–g)** Intensity time traces of the emission from the red and green encircled QDs in panel **e**. The intensity traces can be used to distinguish between QDs that are often in a non/weakly emissive state and positions with a relatively high background level (e.g. due to defects in glass or residual fluorescent organics). "Real" QD positions exhibit characteristic blinking, where the intensity fluctuates between a bright and dark state (e.g. the green spot in **e**, corresponding to the intensity trace in **f**). Intensity traces without such fluctuations are clusters, permanently dim QDs, or spots with a source of constant background intensity (e.g. the red circle in **e**, corresponding to the intensity trace in **g**). The intensity threshold used to distinguish QDs from background signal was set at 3.5 kcounts/25 ms.

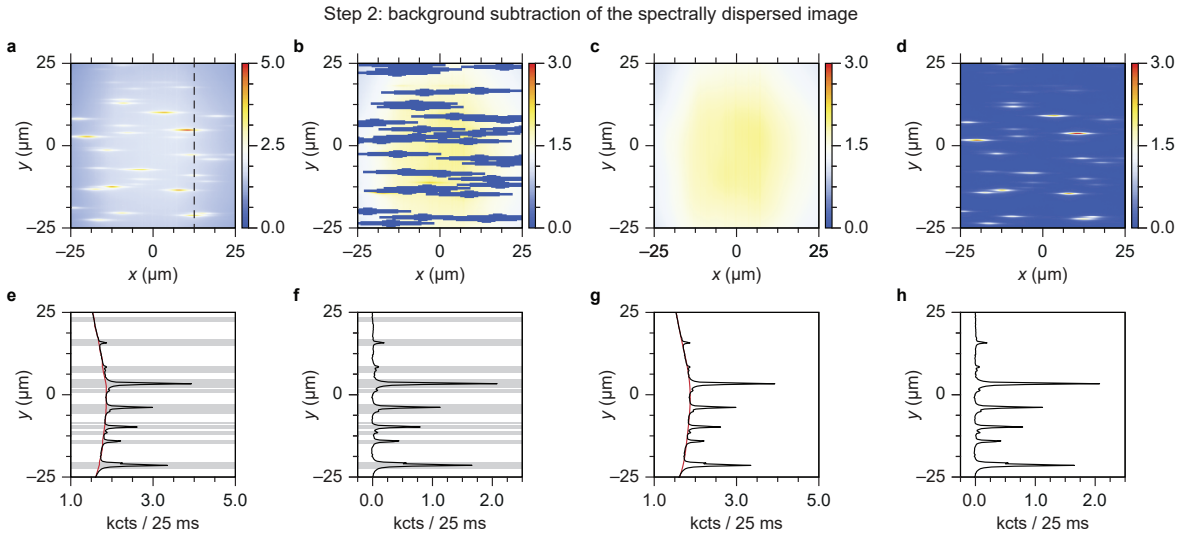

Figure S3 | Procedure of obtaining single-particle emission spectra of CdSe/CdS/ZnS QDs (a) Spectrally dispersed image of the same field of view as in **Figure S2a–d**. Vertical positions of the emission spots remain approximately the same, while the emitted light is dispersed horizontally. Because wide-field excitation but no slit are used in the experiment, various sources of background light contribute to a complex background that may obscure some QD signal. **(b)** Same as **a**, but the regions around identified QD positions (see **d**) are masked. **(c)** Map of the background intensity, calculated using a polynomial fit along each pixel column, excluding pixels that have a higher intensity as a result of spectrally dispersing QD signal (see panels **e–h**). **(d)** Background-corrected, spectrally dispersed image of the emission of multiple QDs. This image serves as the starting point for the analysis of single-particle emission properties. Color scale bars represent average count rates (in kcts/25 ms). **(e)** Vertical cross-cut of the data along the dashed line in **a**), with datapoints corresponding to the masked pixels in panel **b** highlighted by grey shading. These datapoints were excluded as they correspond to regions of higher intensity as a result of QD emission. From the adjusted dataset, a first guess of the background is made by taking a moving average over 25 pixel intensities along the vertical direction (red solid line). **(f)** Same as **e**, but with the guess-background subtracted. The pixels with counts below 100 are selected as pixels unaffected by emission from QDs. These correspond to the unshaded areas and are used to fit the position dependence of the background intensity. **(g)** Same as **e**, but with a one-dimensional 12^{th}-order polynomial fit to the background defined by the selected pixel positions shown in grey in **e–f**. **(h)** Background-corrected cross-section of the dispersed image, obtained by subtracting the polynomial fit to the background.

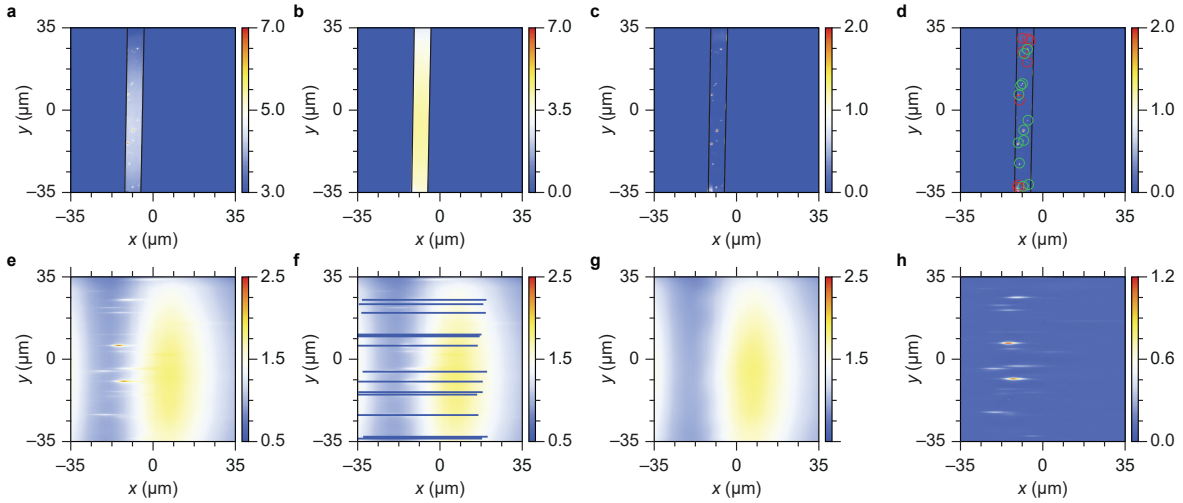

Figure S4 | Multi-particle spectroscopy experiments on InP/ZnSe QDs (a–d) Same as **Figure S2a–d**, but for InP/ZnSe QDs and integrating over 150 s instead of 60 s. To simplify particle identification and to prevent overlapping of potentially broad emission spectra, the image of the field of view was cropped prior to entering the spectrometer (to a horizontal region with a width of ~ 6.5 μm). The intensity threshold used to distinguish QDs from background signal was set at 7.5 kcounts/200 ms. 'False' QD positions are highlighted in red. **(e–h)** Same as **Figure S3a–d**, but using a different masked region (panel **b**) that better corresponds to the signal from the InP/ZnSe QDs. Scale bars represent average count rates (in kcts / 50 ms).

Section S3: Calibration of the emission spectra

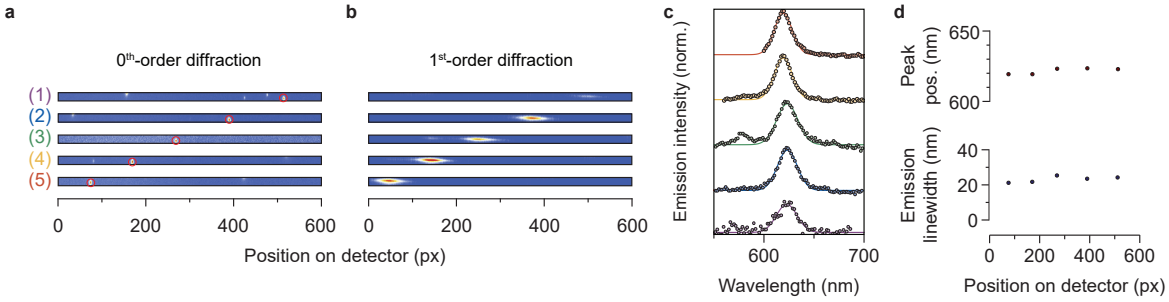

Figure S5 | Calibration of the emission spectra (**a**) Emission from a single CdSe/CdS/ZnS QD, obtained by measuring the image of the 0^{th}-order diffraction. Panels 1–5 are horizontal slices of the 0^{th}-order diffraction image, measured after moving the QD to five different horizontal positions. (**b**) Corresponding horizontal slices of the 1^{st}-order diffraction image (measured without a slit). As a result of moving the QD to five different horizontal positions, the emission spectra are centered at five different horizontal pixel positions of the detector. (**c**) Wavelength-calibrated emission spectra. (**d**) Emission peak wavelength of the QD, measured at five different horizontal positions. (**e**) Same as **d**, but for the emission linewidth (fwhm). Both the QD's emission wavelength and linewidth obtained in our multi-particle spectroscopy setup are independent of the horizontal position of the QD.

Section S4: Particle identification and background subtraction

We observed blinking of the QDs in our experiments. In our analysis of multi-particle spectroscopy data, we ignored frames in which the QD blinked off (or emitted only dimly) by selecting only frames where the fit uncertainties of the emission maximum and line width σ_μ and σ_{fwhm} were below 5 and 40 meV for CdSe/CdS/ZnS QDs, and below 10 and 100 meV for InP/ZnSe QDs. For the CdSe/CdS/ZnS QDs we additionally applied an intensity threshold, selecting only frames where the intensity of a QD was at least 25% of the intensity of its brightest frames.

Section S5: Derivation and fitting of $\langle\Delta^2\rangle$-curves

Due to spectral diffusion (SD), the emission peak energy μ_t fluctuates around the maximum of the time-integrated emission spectrum, μ_{TI}. For random diffusion, the expected mean energy displacement of the emission peak from time t to $t+\tau$ is zero:

$$\langle\Delta\rangle = \langle\mu_t - \mu_{t+\tau}\rangle_t = 0. \tag{1}$$

The mean square energy difference $\langle\Delta^2\rangle$, however, is nonzero:

$$\langle\Delta^2\rangle = \langle[\mu_t - \mu_{t+\tau}]^2\rangle_t > 0. \tag{2}$$

Experimentally, the fitted values of μ_{SF} deviate may from the actual μ^*_{SF} due to Poisson noise, or a non-Gaussian shape of the emission spectrum. As a result, the experimentally obtained $\langle\Delta^2\rangle$-curve can be expressed as

$$\langle\Delta^2\rangle = \int \left[\mu_t - \mu_{t+\tau}\right]^2 e^{-\left[\mu_t - \mu^*_{SF}\right]^2/2\sigma^2} e^{-\left[\mu_{t+\tau} - \mu^*_{SF} + d\mu\right]^2/2\sigma^2} e^{-d\mu^2/2\delta^2} d\mu_t d\mu_{t+\tau} d(d\mu) = \delta^2 + 2\sigma^2, \tag{3}$$

where δ^2 is the SD-induced mean square energy difference for emission spectra recorded at different times, and σ is the error on the emission maximum. The magnitude of σ is 1.9 ± 0.8 meV and 3.2 ± 1.1 meV for the experiments on CdSe/CdS/ZnS and InP/ZnSe, respectively (see Figure S7a,c). The $\langle\Delta^2\rangle$-curves in Figure 2l (main text) thus contain the information about the dynamics of SD and are vertically offset by a finite value of σ.

We fitted experimental $\langle\Delta^2\rangle$-curves, obtained with 100-ms binning, to the equation

$$\langle\Delta^2\rangle = \Delta^2_\infty\left(1 - e^{-\tau/t_c}\right) + 2\sigma^2, \tag{4}$$

using all datapoints up to a delay time of 12 s with weights $\frac{\sqrt{N_i}}{\sigma_{\Delta_i^2}} \log\left(\frac{\tau_i}{\tau_{i+1}}\right)$. Here, τ_i is the delay time of data point i, N_i is the number of pairs of frames that contributed and $\sigma_{\Delta_i^2}$ is the error on the data point. We used the logarithmic term to compensate for the fact that there are few data point at small delay times τ and more at longer delays. We fixed the value of $2\sigma^2$ using the mean fit uncertainty of the emission maximum of the respective QD.

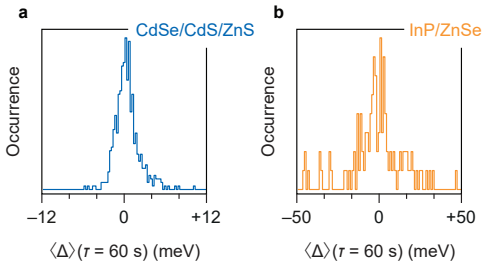

Figure S6 | Characterization of sample drift. (**a**) Histogram of $\langle\Delta\rangle$ (τ = 60 s), for all CdSe/CdS/ZnS QDs. In our multi-particle spectroscopy experiments, sample drift should manifest itself as a systematic shift of all QD spectra (positions) to higher/lower energies (left/right). However, as the histogram of the mean energy difference is approximately symmetric around $\langle\Delta\rangle = 0$ meV, we conclude that there is no significant sample drift at the timescale of our measurements. (**b**) Same, but for the InP/ZnSe QDs.

Section S6: Rotational diffusion model for spectral diffusion

We consider a model of a spherical QD in which the lowest-energy exciton state has a static dipole moment $\mathbf{p}$ due an off-center core or off-center localization of a charge carrier. The first-order correction to the exciton energy due to the presence of an elementary charge on the QD surface is

$$E = \frac{q}{4\pi\varepsilon\varepsilon_0}\frac{\mathbf{p}\cdot\mathbf{r}}{r^3}, \tag{5}$$

where $\mathbf{r}$ is the location of the charge and ε the relative permittivity of the QD material. This expression neglects dielectric contrast between the QD and its surroundings. If we align the z-axis of our coordinate system with $\mathbf{p}$ and express $\mathbf{r}$ in spherical coordinates with r equal to the QD radius a, the energy correction depends only on the polar angle θ:

$$E(\theta) = \frac{q}{4\pi\varepsilon\varepsilon_0}\frac{p\cos\theta}{a^2}. \tag{6}$$

As the simplest possible model of spectral diffusion, we consider the effect of a single charge of fixed magnitude q diffusing over the spherical QD surface. The movement is described in terms of the probability density $f(\theta, \varphi, t)$ to encounter the charge at location (θ, φ) at time t, which obeys

$$D_{\mathrm{rot}}\nabla^2 f = \frac{\partial f}{\partial t}, \tag{7}$$

where D_{rot} is the rotational diffusion constant. The general solution to this differential equation is

$$f(\theta, \varphi, t) = \sum_{l=0}^{\infty}\sum_{m=-l}^{l} C_{lm} Y_l^m(\theta, \varphi)\mathrm{e}^{-D_{\mathrm{rot}} l(l+1)t}, \tag{8}$$

where Y_l^m are the spherical harmonics and C_{lm} are expansion coefficients determined by boundary conditions. We see that only the term with $l = 0$ survives as t approaches infinity, yielding a uniform distribution $f(\theta, \varphi, t)$. If f is a Dirac delta function at location (θ_0, φ_0) at $t = 0$, then the expansion coefficients are

$$C_{lm} = \int_0^{2\pi}\int_0^{\pi} Y_l^{m^*}(\theta, \varphi) f(\theta, \varphi, 0)\sin\theta\,\mathrm{d}\theta\mathrm{d}\varphi = Y_l^{m*}(\theta_0, \varphi_0), \tag{9}$$

yielding an expression for the more general probability density to encounter the charge at location (θ, φ) at time t given that it was at location (θ_0, φ_0) at time $t = 0$:

$$f(\theta, \varphi, t \mid \theta_0, \varphi_0) = \sum_{l=0}^{\infty}\sum_{m=-l}^{l} Y_l^{m*}(\theta_0, \varphi_0) Y_l^m(\theta, \varphi)\mathrm{e}^{-D_{\mathrm{rot}} l(l+1)t}, \tag{10}$$

We obtain spectral-diffusion statistics and dynamics by averaging $E(\theta)$ and $E^2(\theta)$ over the probability density $f(\theta, \varphi, t \mid \theta_0, \varphi_0)$. We will use that

$$E(\theta) = \frac{q}{4\pi\varepsilon\varepsilon_0}\frac{p}{a^2}\sqrt{\frac{4\pi}{3}}Y_1^0(\theta, 0), \tag{11}$$

$$E(\theta)^2 = \left(\frac{q}{4\pi\varepsilon\varepsilon_0}\frac{p}{a^2}\right)^2\left[\sqrt{\frac{16\pi}{45}}Y_2^0(\theta, 0) + \sqrt{\frac{4\pi}{9}}Y_0^0(\theta, 0)\right], \tag{12}$$

and the orthonormality of the spherical harmonics. This means that from the expansion of f only terms with $l \leq 2$ and $m = 0$ contribute to spectral diffusion.

If the charge starts at (θ_0, φ_0) and then evolves as described by $f(\theta, \varphi, t \mid \theta_0, \varphi_0)$, the energy correction starts at $E_0 = E(\theta_0)$ and then evolves as

$$\langle E\rangle_\Omega = \int_0^{2\pi}\int_0^{\pi} E(\theta) f(\theta, \varphi, t \mid \theta_0, \varphi_0)\sin\theta\,\mathrm{d}\theta\mathrm{d}\varphi = \frac{q}{4\pi\varepsilon\varepsilon_0}\frac{p}{a^2}\sqrt{\frac{4\pi}{3}}Y_1^0(\theta_0, 0)\,\mathrm{e}^{-2D_{\mathrm{rot}}t} = E(\theta_0)\,\mathrm{e}^{-2D_{\mathrm{rot}}t}, \tag{13}$$

where $\langle\cdot\rangle_\Omega$ denotes averaging over all possible locations (θ, φ) of the charge at time t. Similarly, the square of the energy correction evolves as

$$\langle E^2\rangle_\Omega = \left(\frac{q}{4\pi\varepsilon\varepsilon_0}\frac{p}{a^2}\right)^2\left[\sqrt{\frac{16\pi}{45}}Y_2^0(\theta_0, 0)\,\mathrm{e}^{-6D_{\mathrm{rot}}t} + \sqrt{\frac{4\pi}{9}}Y_0^0(\theta_0, 0)\right] = \left[E(\theta_0)^2 - E_\infty^2\right]\mathrm{e}^{-6D_{\mathrm{rot}}t} + E_\infty^2, \tag{14}$$

where in the last step we have introduced

$$E_\infty^2 = \frac{1}{3}\left(\frac{q}{4\pi\varepsilon\varepsilon_0}\frac{p}{a^2}\right)^2. \tag{15}$$

Now we can average the above two expressions over the uniform distribution of possible initial charge locations θ_0:

$$\langle E\rangle_{\Omega,\Omega_0} = \frac{1}{2}\int_0^\pi \langle E\rangle_\Omega \, \sin\theta_0 \, \mathrm{d}\theta_0 = 0 \tag{16}$$

$$\langle E^2\rangle_{\Omega,\Omega_0} = \frac{1}{2}\int_0^\pi \langle E^2\rangle_\Omega \, \sin\theta_0 \, \mathrm{d}\theta_0 = E_\infty^2 \tag{17}$$

And finally:

$$\langle E_t E_0\rangle_{\Omega,\Omega_0} = \frac{1}{2}\int_0^\pi \langle E\rangle_\Omega E(\theta_0) \, \sin\theta_0 \, \mathrm{d}\theta_0 = E_\infty^2 \, \mathrm{e}^{-2D_{\mathrm{rot}}t} \tag{18}$$

With the above expressions, we can calculate the mean squared energy shift due to spectral diffusion as a function of delay time t between spectral measurements:

$$\langle (E_t - E_0)^2\rangle_{\Omega,\Omega_0} = \langle E_t^2\rangle - 2\langle E_t E_0\rangle + \langle E_0^2\rangle = 2E_\infty^2\left(1 - \mathrm{e}^{-2D_{\mathrm{rot}}t}\right) \tag{19}$$

Section S7: Origin of weak and positive correlations between emission energy and linewidth

Part of the QDs do not show spectral diffusion (SD) with a clear negative correlation between their emission energy and linewidth. Specifically, 29.7% of the CdSe/CdS/ZnS and 23.1% of the InP/ZnSe QDs exhibit SD with a Pearson correlation coefficient $-0.25 < \rho_{\mu,\mathrm{fwhm}} < +0.25$. Figure S6 shows the relationship between the variations in single-frame peak energy and linewidth that are exhibited by QDs with different values of $\rho_{\mu,\mathrm{fwhm}}$. No clear correlation is apparent between the value of $\rho_{\mu,\mathrm{fwhm}}$ and the magnitude of SD-induced fluctuations of the single-frame emission energy and linewidth for either the CdSe/CdS/ZnS and InP/ZnSe QDs.

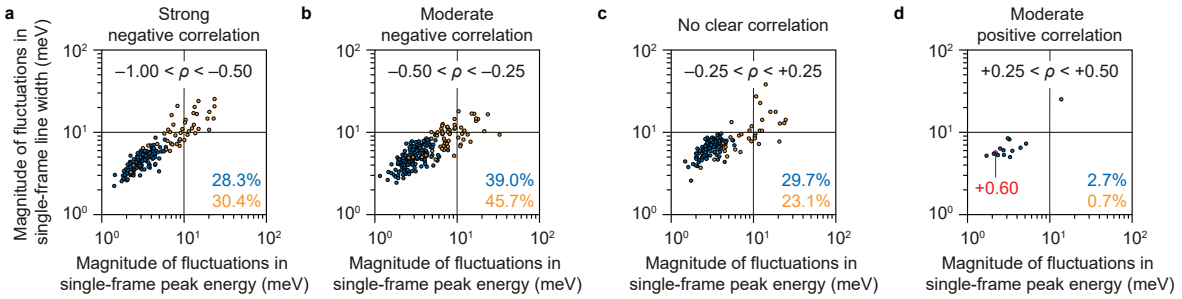

Figure S7 | Magnitude of spectral diffusion-induced fluctuations for different correlations between μ_{SF} and $\mathrm{fwhm}_{\mathrm{SF}}$. (**a**) Magnitude of single-particle fluctuations in emission peak energy μ_{SF} and linewidth $\mathrm{fwhm}_{\mathrm{SF}}$ for the majority of QDs that show a strong negative correlation between μ_{SF} and $\mathrm{fwhm}_{\mathrm{SF}}$ ($-1.00 < \rho_{\mu,\mathrm{fwhm}} < -0.50$). (**b–d**) Same, but for moderate negative correlations ($-0.50 < \rho_{\mu,\mathrm{fwhm}} < -0.25$), unclear correlations ($-0.25 < \rho_{\mu,\mathrm{fwhm}} < +0.25$) and moderate positive correlations ($+0.25 < \rho_{\mu,\mathrm{fwhm}} < +0.50$). Each data point in panel **a–d** represents an individual QD. Results for CdSe/CdS/ZnS (blue) and InP/ZnSe (yellow) are shown in the same plots.

Figure S8 shows histograms of the spread (standard deviation) and average fit uncertainties of the emission peak energy μ_{SF} and linewidth $\mathrm{fwhm}_{\mathrm{SF}}$, for different values of $\rho_{\mu,\mathrm{fwhm}}$. For both the CdSe/CdS/ZnS and the InP/ZnSe QDs, the SD-induced variations of the emission peak energy and line width are larger than the associated fit uncertainties. We observe that the fit uncertainties are typically larger for the QDs where we did not see a clear negative correlation between μ_{SF} and $\mathrm{fwhm}_{\mathrm{SF}}$.

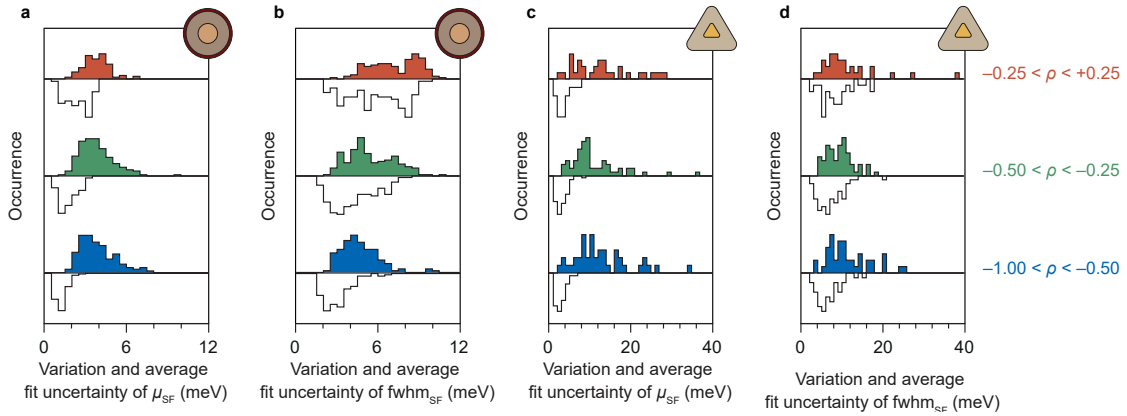

Figure S8 | Impact of fit uncertainties on the correlated behavior between μ_{SF} and $\mathrm{fwhm}_{\mathrm{SF}}$. (**a**) Histogram of the SD-induced variation (standard deviation; colored histograms) and average fit uncertainties (open histograms, upside-down) of the emission peak energy μ_{SF} for the measurements on CdSe/CdS/ZnS QDs. The different colors correspond to QDs with strongly negative, moderate negative, and unclear correlations between μ_{SF} and $\mathrm{fwhm}_{\mathrm{SF}}$, as indicated by the values of $\rho_{\mu,\mathrm{fwhm}}$. (**b**) Same, but for the variation and fit uncertainty of the emission line width $\mathrm{fwhm}_{\mathrm{SF}}$. (**c–d**) Same as **a–b**, but for the InP/ZnSe QDs.

A minor fraction (2.7%) of the CdSe/CdS/ZnS QDs displayed a weak positive emission energy–line width correlation ($+0.25 < \rho_{\mu,\mathrm{fwhm}} < +0.50$). One QD (0.2%) exhibited a strong positive correlation with $\rho_{\mu,\mathrm{fwhm}} > +0.50$. Upon closer inspection of these 13 QDs, we find that these positive correlations do not represent intrinsic photophysics of the QDs as they have come about due to either (1) an experimental artefact that occurs when two QDs are spaced closely together (see Figure S9a–b), (2) imperfect background subtraction of the emission spectrum for weakly-emitting QDs, or (3) photodegradation of the QD that leads to a gradual blueshift of the emission spectrum[S1,S2] (see Figure 9c–d).
The experimental artefact occurs when two QDs are spaced closely together leading to overlap of the emission spectra in the 1st-order diffraction image (see e.g. Figure S9a–b). Since the wavelength calibration (see Figure 1e–f, main text) is based on the position of one selected QD, overlap of two emission spectra leads to a shoulder in the emission spectrum that originates from emission of the neighboring QD, either on the red or blue side of the actual emission spectrum. At times when the selected QD emits weakly, emission signal from a blue (red) neighboring QD will lead to a Gaussian fit with a blue-shifted (red-shifted) center wavelength and a broadened emission spectrum. As a strategy to minimize the occurrence of this experimental artefact, we fitted only to the wavelength region around the relevant emission peak. As such, the actual emission spectrum of the selected QD is at most affected by a shoulder of a neighboring QD.

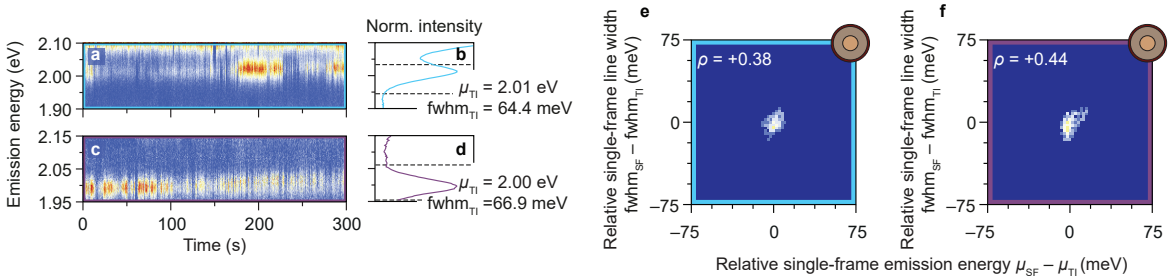

Figure S9 | Quantum dots exhibiting a 'false' positive correlation between μ_{SF} and fwhm$_{SF}$. (**a**) Example of a result from a multi-particle spectroscopy experiment where emission from a QD was measured while spaced closely together with another QD. Since the wavelength calibration (see Figure 1e–f, main text) is based on the position of one selected QD, overlap of two emission spectra leads to a shoulder in the emission spectrum that originates from emission of the neighboring QD. In this case the contribution of the neighboring QD adds a shoulder on the blue side of the actual emission spectrum. At times when the selected QD emits weakly, emission signal from this blue (red) ghost QD will lead to a Gaussian fit with a blue-shifted (red-shifted) center wavelength and a broadened emission spectrum. (**b**) Time-integrated emission spectrum of the actual and ghost QD (solid black line), and histogram of the fitted emission peak energies (colored histogram). As a strategy to minimize the occurrence of the experimental artefact, we selected only the wavelength region around the emission peak to be fitted with a Gaussian. As such, the fit of the emission spectrum of the selected QD is at most affected by a shoulder of a neighboring QD's emission spectrum. (**c–d**) Same as **a–b**, but for a QD that exhibits photodegradation. A characteristic gradual blue shift is apparent in the emission time trace. (**e–f**) Correlation between the single-frame (100 ms) emission energy and line width, μ_{SF} and fwhm$_{SF}$. The correlations are shown as 2D histograms of μ_{SF} and fwhm$_{SF}$, relative to the time-integrated peak energy and line width, for the QDs in a–d (same colors).

Section S8: Structural characterization of CdSe/CdS/ZnS QDs

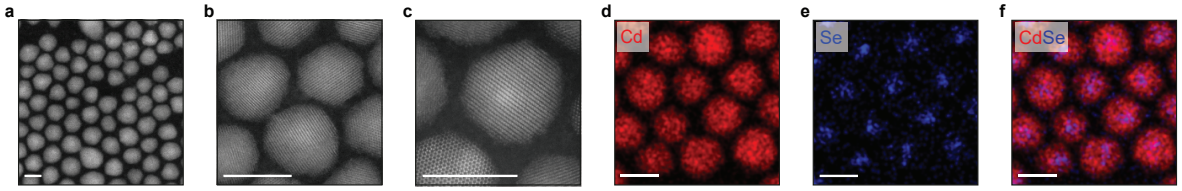

Figure S10 | Structural characterization of CdSe/CdS/ZnS QDs (**a–c**) HAADF-STEM images of the CdSe/CdS/ZnS QDs. The CdSe core appears slightly more bright than the CdS shell. (**d–f**) EDX net count maps of the elements Cd (red) and Se (blue), shown separately in **d** and **e**, and overlaid in **f**. Scale bars are 10 nm.

Section S9: Correlation between emission energy and single-frame emission line width

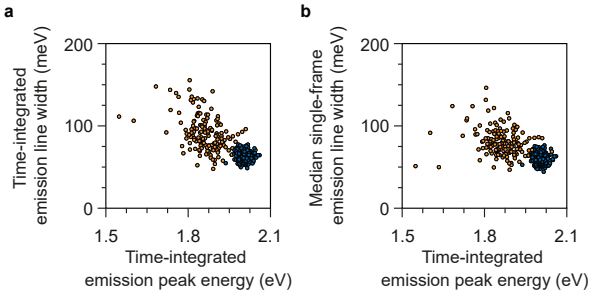

Figure S11 | Correlations in single-particle emission properties. (**a**) Correlation between the time-integrated emission peak energy and line width. (**a**) Correlation between the time-integrated emission peak energy and the single-frame (100 ms) emission line width.

Supporting References

(S1) Nirmal, M.; Dabbousi, B.O.; Bawendi, M.G.; Macklin, J.J.; Trautman, J.L.; Harris, T.D.; Brus, L.E.; Fluorescence Intermittency in Single Cadmium Selenide Nanocrystals, *Nature* **1996**, *383*, 802–804.

(S2) Van Sark, W.G.J.H.M.; Frederix, P.L.T.M.; Bol, A.A.; Gerritsen, H.C.; Meijerink, A.; Blueing, Bleaching, and Blinking of Single CdSe/ZnS Quantum Dots, *ChemPhysChem* **2002**, *3*, 871–879.